SUPPORTING INFORMATION

Redox-Driven *In Situ* Helix Reversal of Graphene-Based Hydrogels

Yaqian Zhang, Minggao Qin, Chao Xing, Changli Zhao, Xiaoqiu Dou, Chuanliang Feng*

State Key Lab of Metal Matrix Composites, School of Materials Science and Engineering, Shanghai Jiao Tong University, 800 Dongchuan Road, Shanghai, P. R. China, 200240

*Corresponding author

Tel: 86 2154747651; E-mail: clfeng@sjtu.edu.cn

S1. Characterization of GO

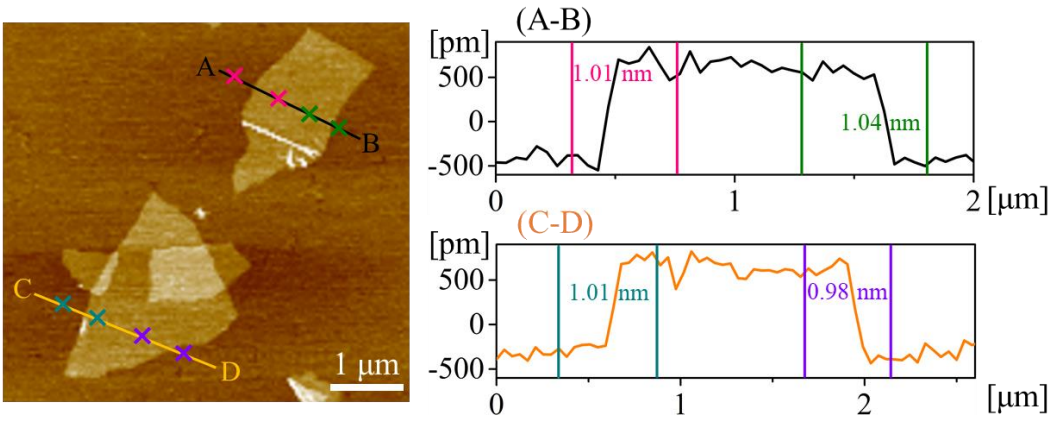

Figure S1. AFM image of GO sheets.

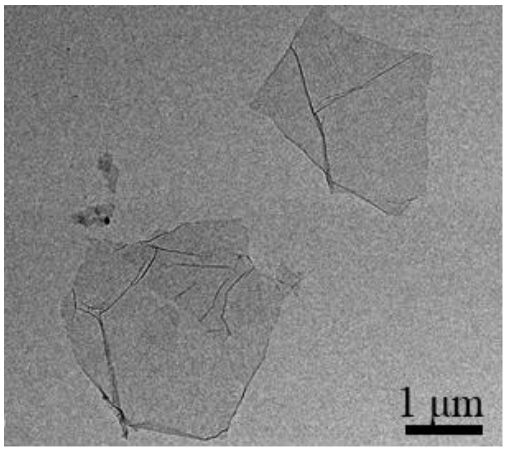

Figure S2. TEM image of GO sheets.

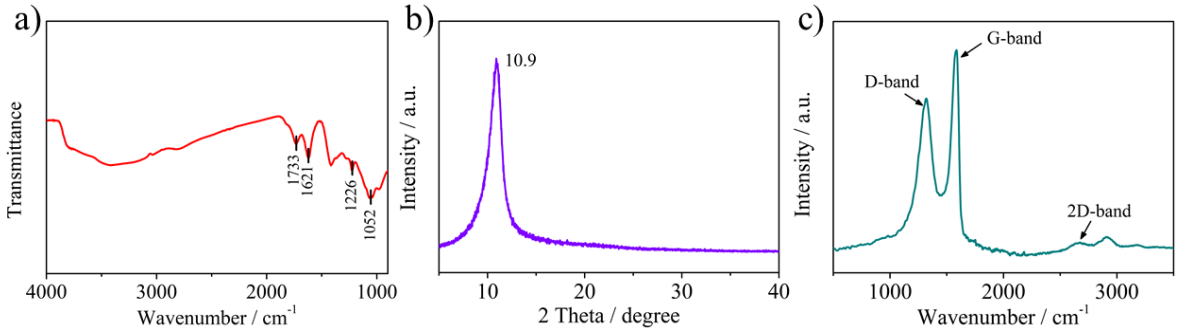

Figure S3. (a) FTIR, (b) XRD and (c) Raman spectra of GO.

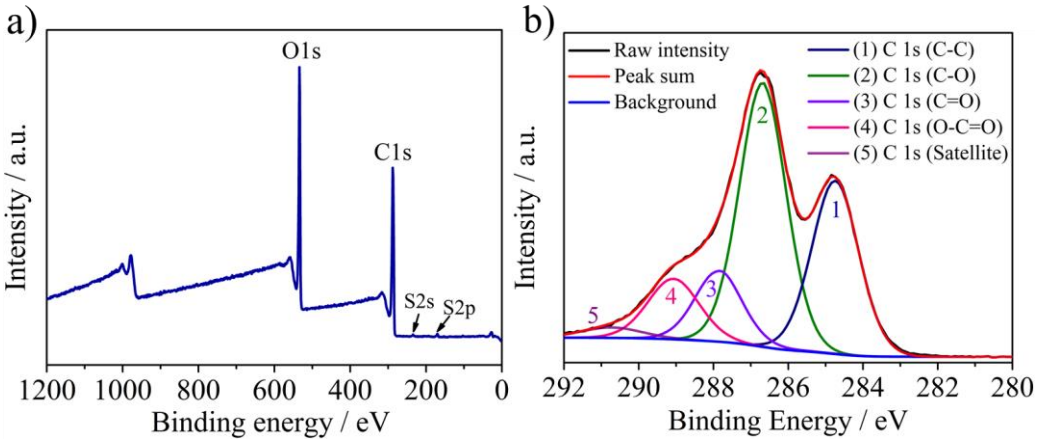

Figure S4. (a) XPS survey spectrum of GO. (b) Typical high-resolution XPS spectrum of C 1s region of GO.

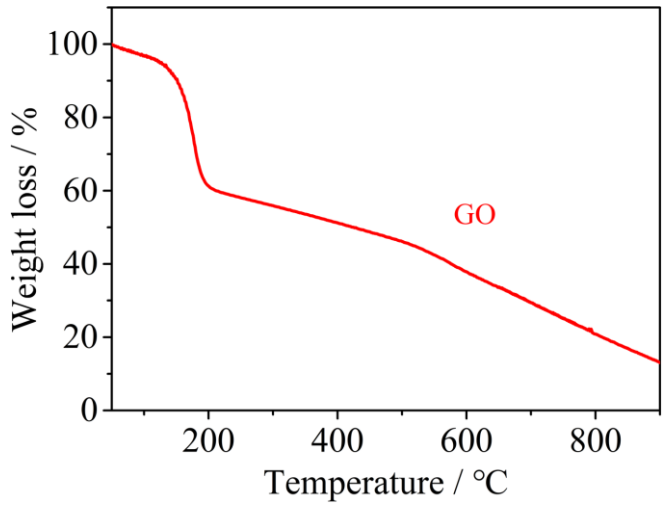

Figure S5. TGA plots of GO.

S2. Morphologies of L/DPFEG xerogels

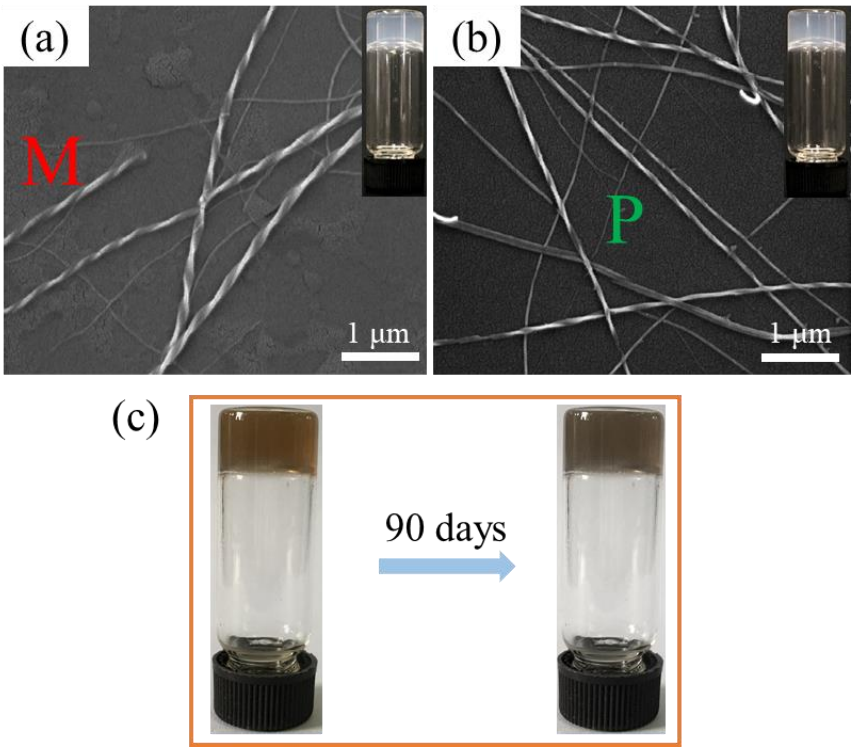

Figure S6. SEM images and photographs of (a) LPFEG and (b) DPFEG hydrogels. (c) The stability of LPFEG-GO hydrogel with three-month storage.

S3. Rheological properties of LPFEG-GO hydrogels

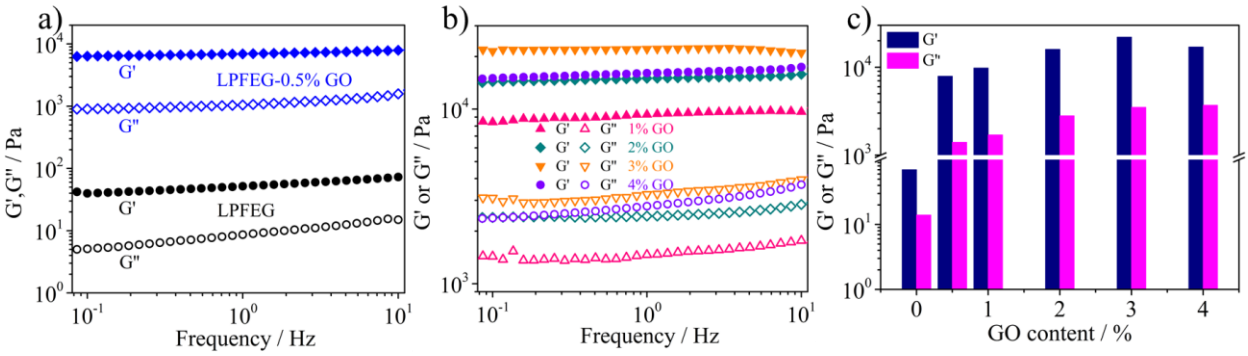

Figure S7. (a, b) Rheological properties of LPFEG-GO hydrogels with different amount of GO. (c) Comparison of the storage modulus (G') and loss modulus (G″) for the LPFEG-GO hydrogels with different amount of GO.

S4. Chiroptical properties of DPFEG and DPFEG-GO hydrogels

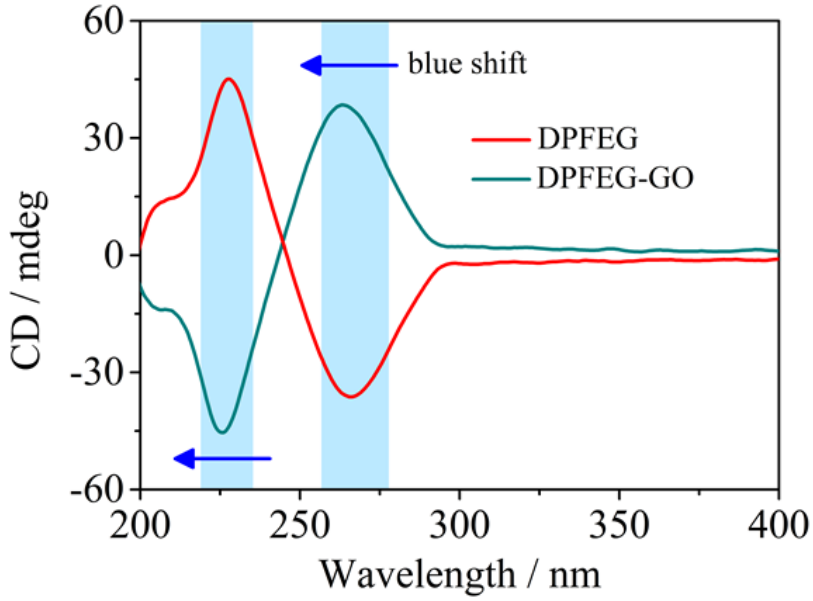

Figure S8. CD spectra of DPFEG and DPFEG-GO gels.

S5. Molecular chirality of L/DPFEG

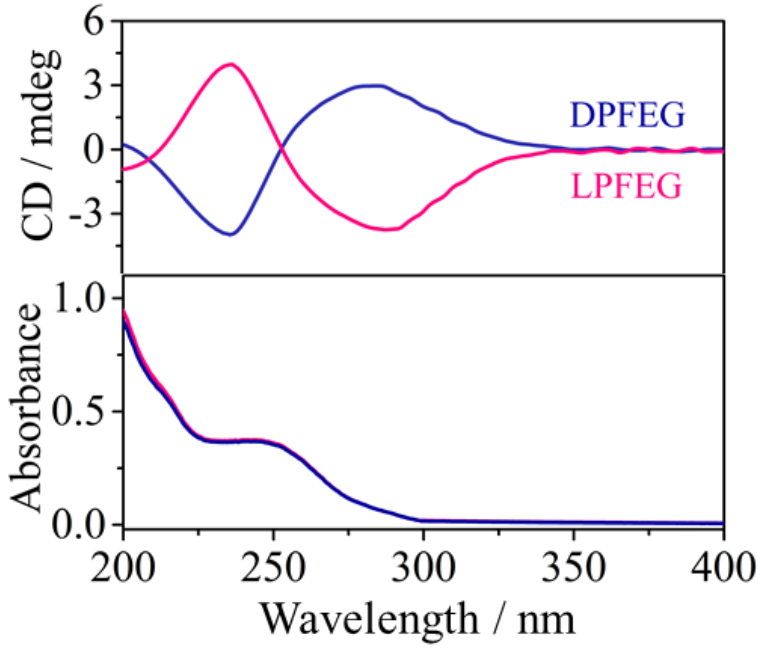

Figure S9. CD spectra and corresponding UV absorption of LPFEG and DPFEG (0.02 mg/mL) in molecularly ethanol solution.

S6. Photographs of LPFEG-GO and LPFEG hydrogels

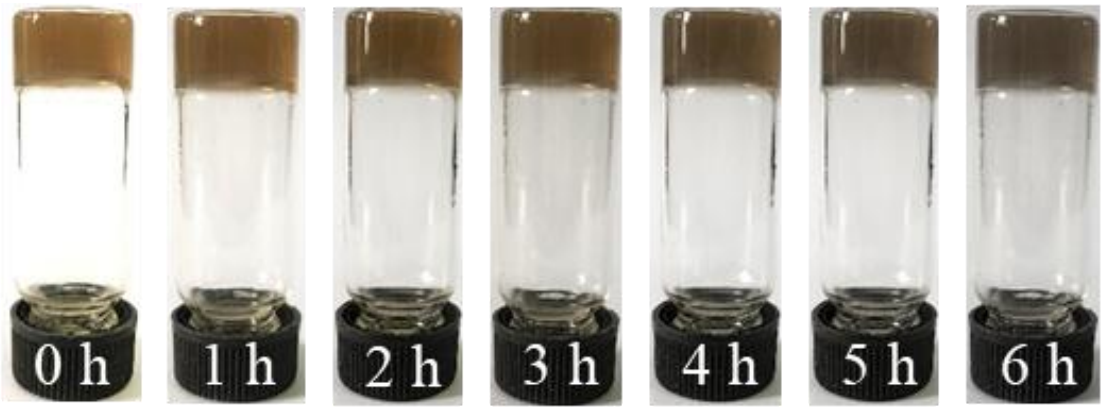

Figure S10. Photographs of LPFEG-GO hydrogel under UV light irradiation with different time intervals.

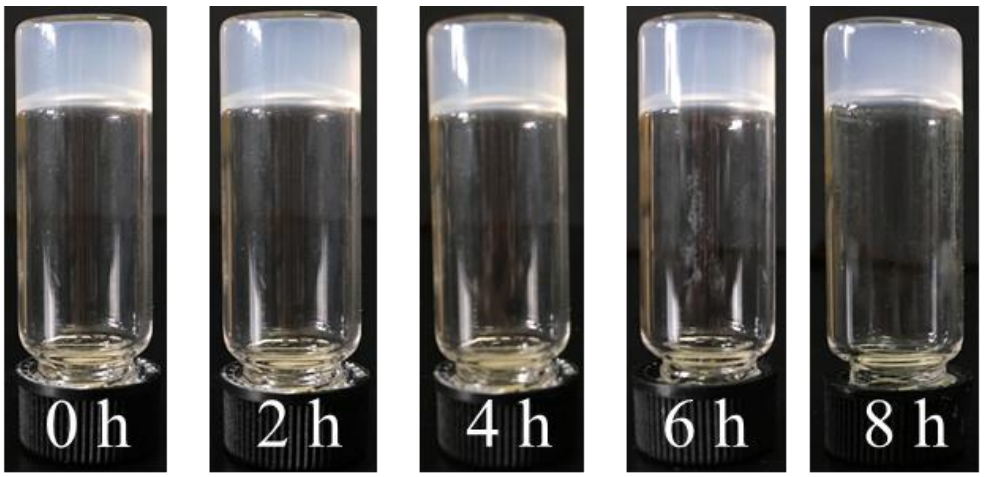

Figure S11. Photographs of LPFEG hydrogel under UV light irradiation with different time intervals.

S7. Irradiation-dependent spectral changes of L/DPFEG-GO hydrogels

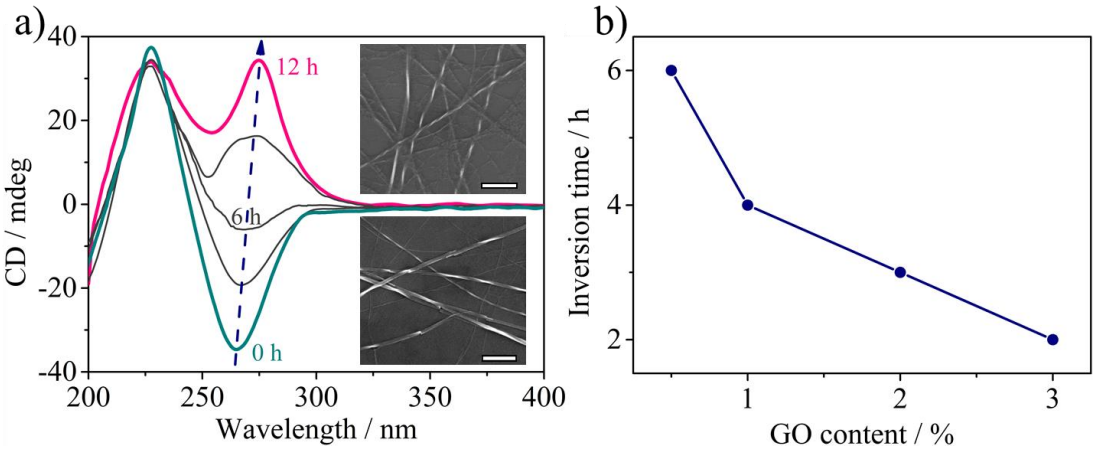

Figure S12. (a) UV irradiation-dependent CD spectral changes of LPFEG-GO hydrogel with 0.5 wt% addition of GO. The insets showed the corresponding SEM images before and after 12 h of irradiation (Scale bar: 1 μm). (b) The irradiation time required for chirality inversion of LPFEG-GO hydrogels with different GO contents.

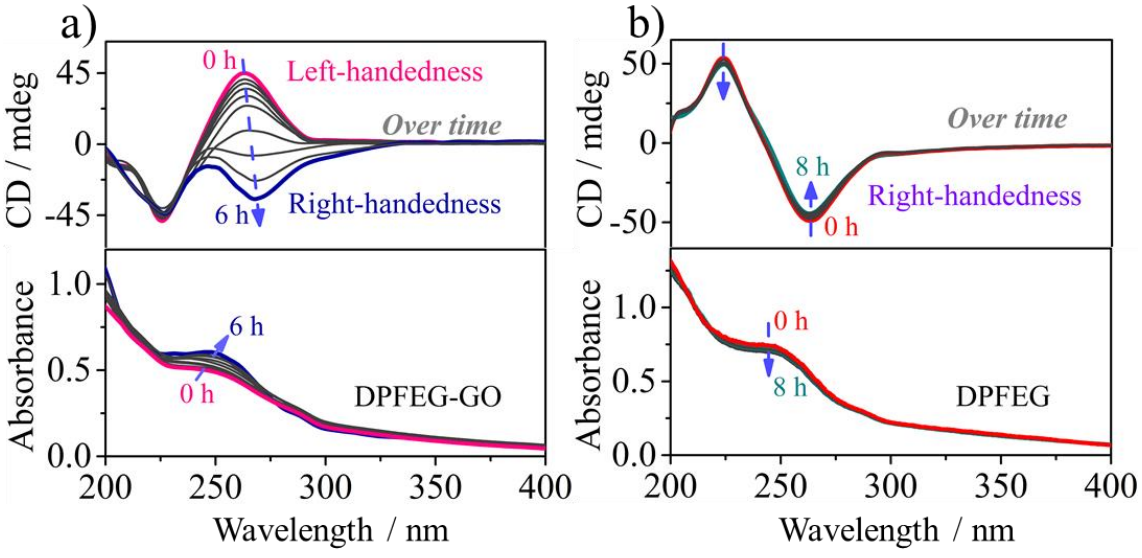

Figure S13. UV irradiation-dependence CD and corresponding absorption spectral changes of (a) DPFEG-GO and (b) DPFEG.

S8. Raman spectra of LPFEG-GO xerogel

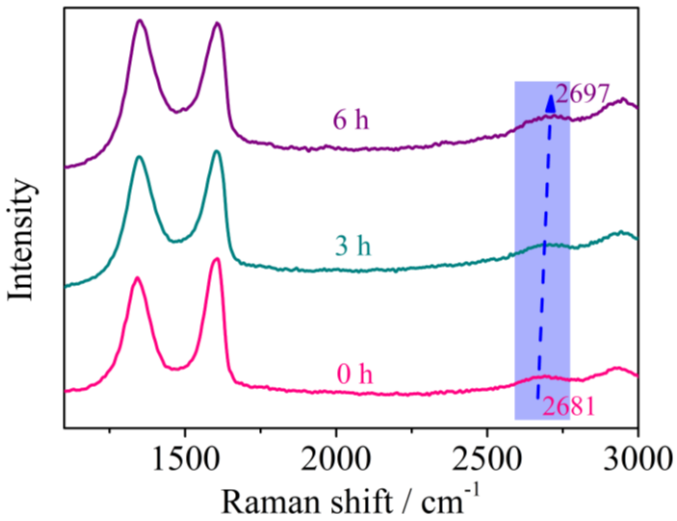

Figure S14. Raman spectra of LPFEG-GO assemblies with different irradiation time in the range 1100-3000 cm^{-1}.

S9. Time-dependent morphology changes of L/DPFEG-GO and L/DPFEG hydrogels

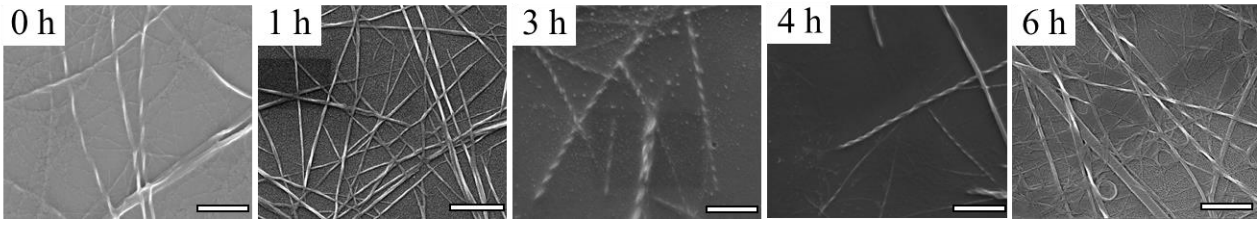

Figure S15. Time-dependent SEM images of LPFEG-GO gel with extension of UV light irradiation (Scale bar: 1 μm).

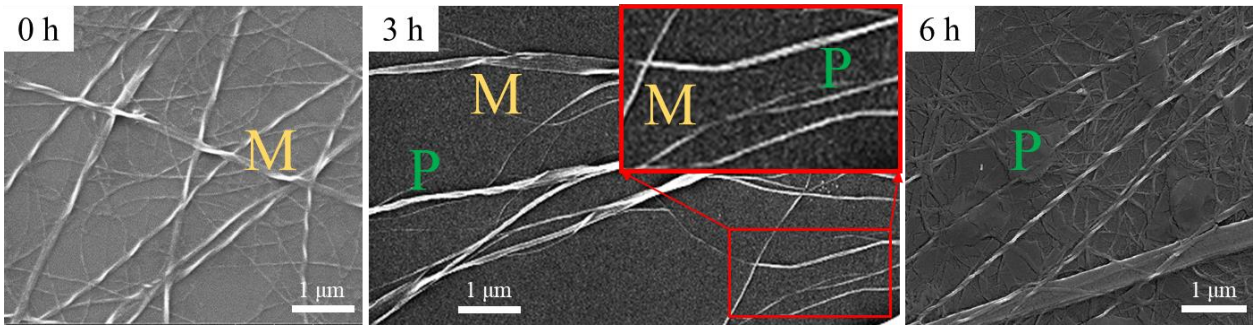

Figure S16. Time-dependence SEM images of DPFEG-GO gel with extension of UV light irradiation.

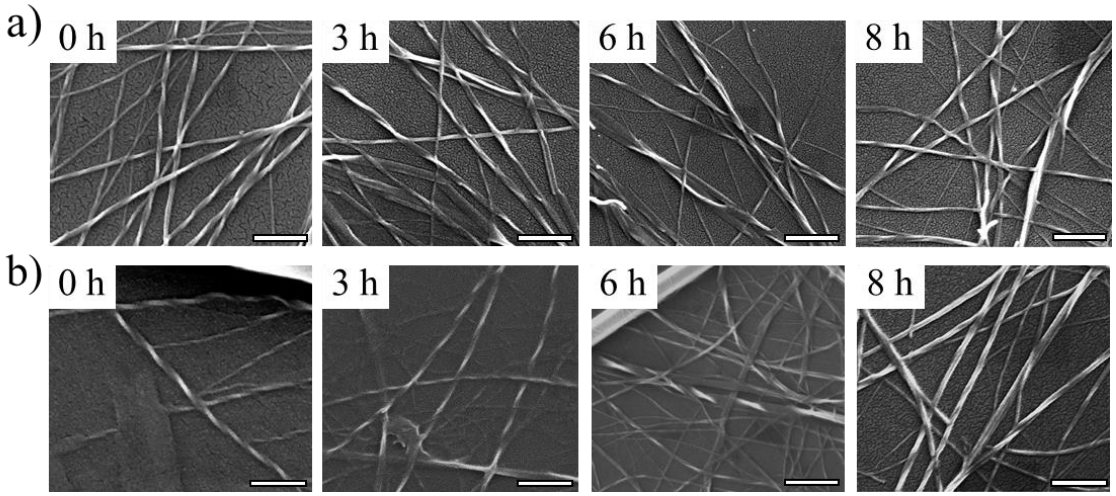

Figure S17. Time-dependent SEM images of LPFEG (a) and DPFEG (b) hydrogels with extension of UV light irradiation (Scale bar: 1 μm).

S10. Irradiation-dependent ^{1}H NMR spectra of LPFEG hydrogel

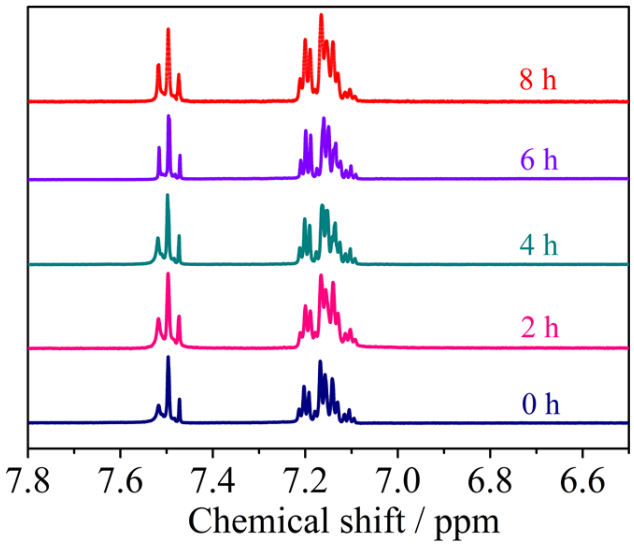

Figure S18. Time-dependence ^{1}H NMR spectra of LPFEG gel assembled in D_2O with extension of UV light irradiation.

S11. Assembly morphologies of LPFEG xerogels

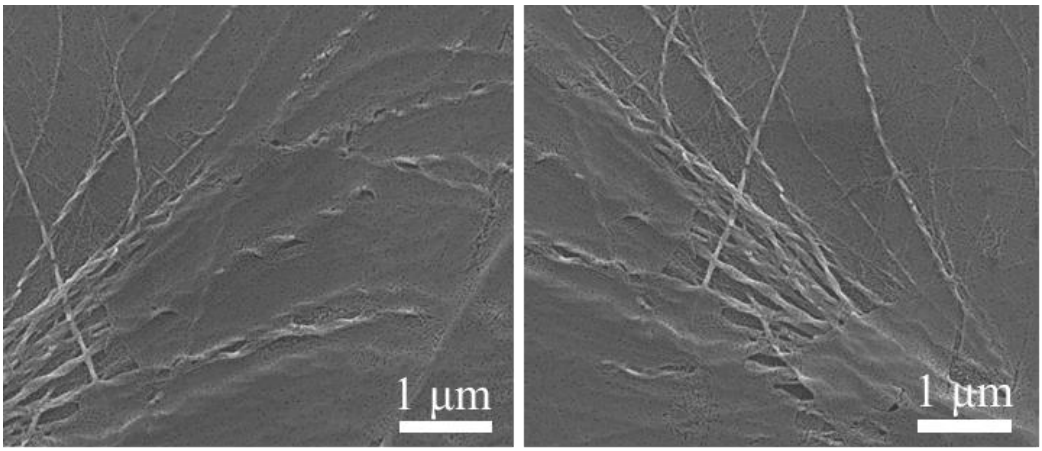

Figure S19. SEM images of LPFEG assembled on GO surface (left) and RGO surface (right).

S12. XRD spectral changes of GO membrane

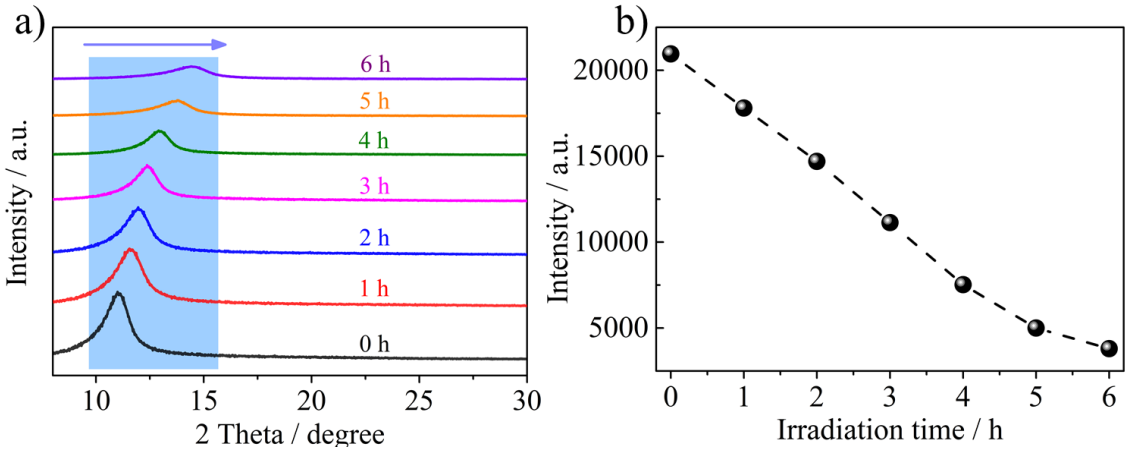

Figure S20. (a) XRD spectra of GO membrane prepared by UV irradiation for different time. (b) The intensity evolution of the characteristic diffraction peak.

S13. Temperature-dependent ^{1}H NMR spectra of LPFEG hydrogel

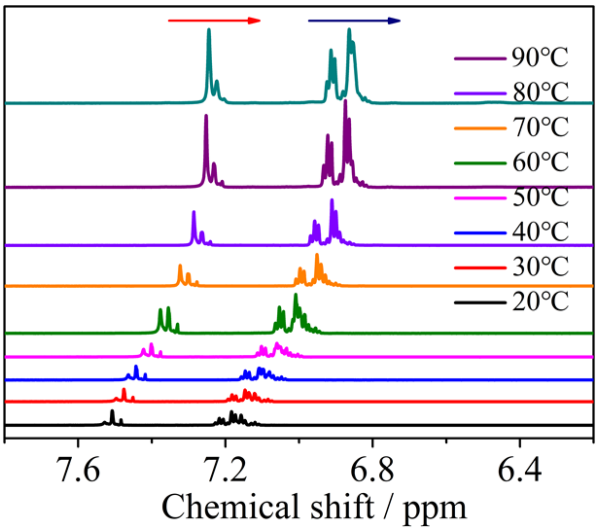

Figure S21. Temperature-dependent ^{1}H NMR spectra of LPFEG gel assembled in D_2O.

S14. Variations in CD spectra of LPFEG-GO hydrogel

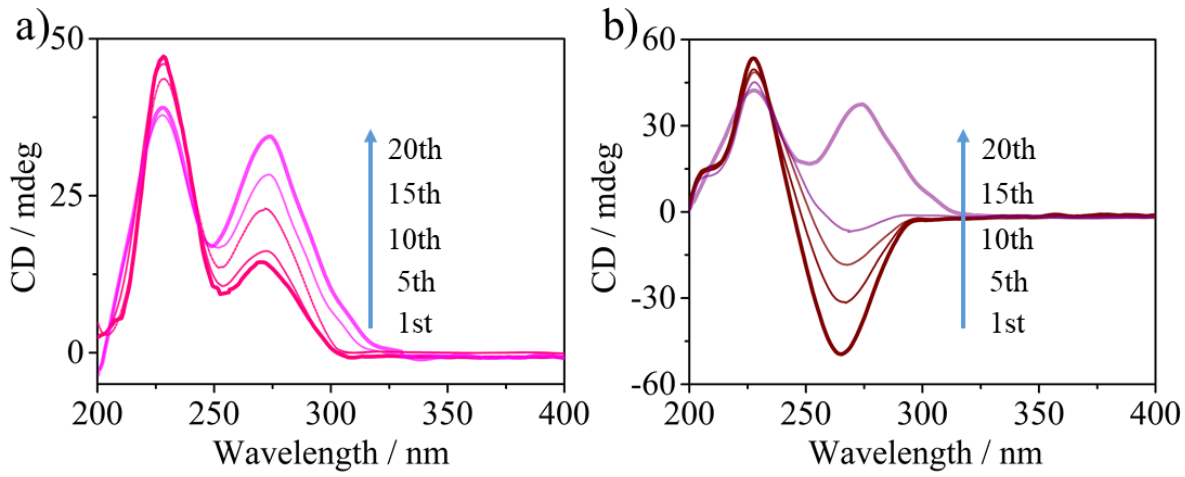

Figure S22. Variations in CD spectra of LPFEG-GO gel at each a) 20°C and b) 80°C of various heating/cooling cycles.

S15. Shape memory behaviors of LPFEG-GO membrane

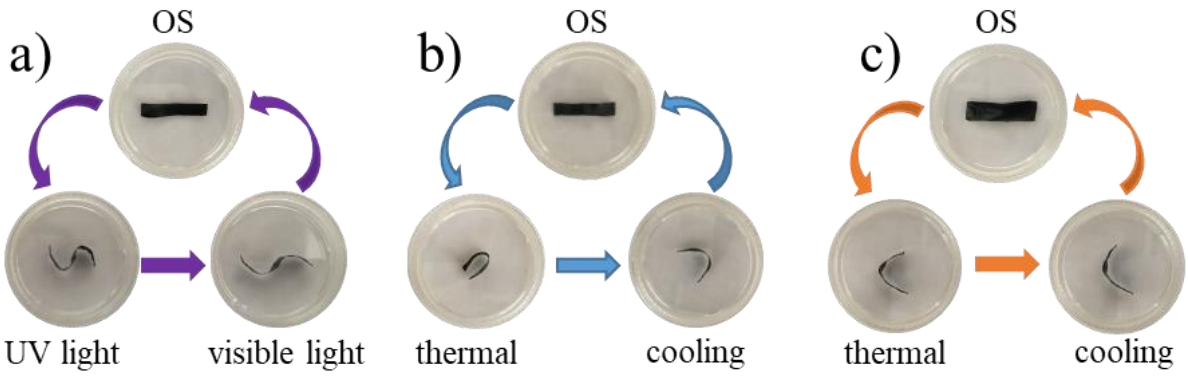

Figure S23. The a) irradiation and b, c) temperature-induced shape memory behaviors based on LPFEG-GO membrane. “OS” refers to “original shape”.

S16. Photographs of LPFEG-GO membrane

Figure S24. Time-dependent changes in LPFEG-GO membrane employing for drug-release process.

S17.

S17. UV-vis spectra of DP and NS before and after absorption

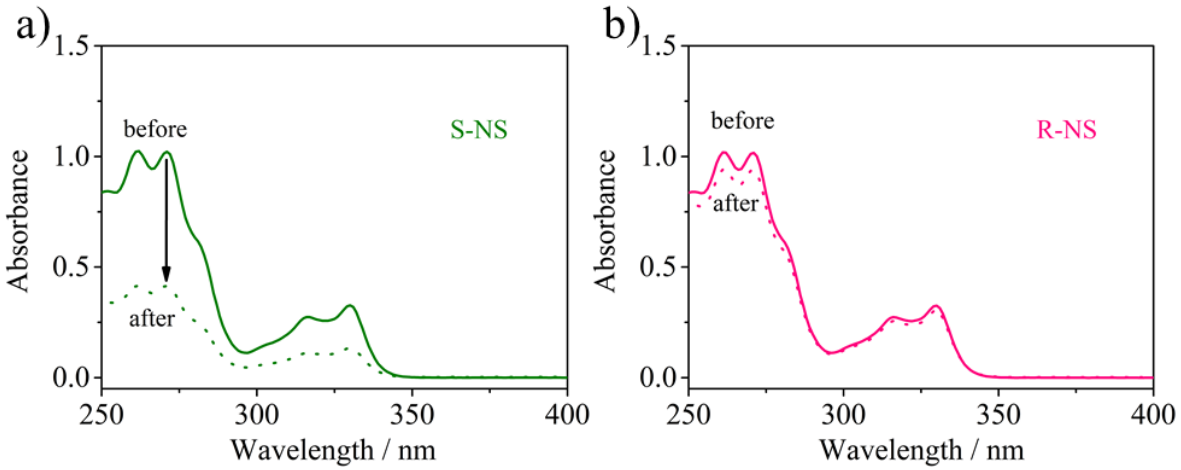

Figure S25. UV-vis spectra of (a) S-NS and (b) R-NS solutions before and after absorption employing LPFEG-GO membrane.

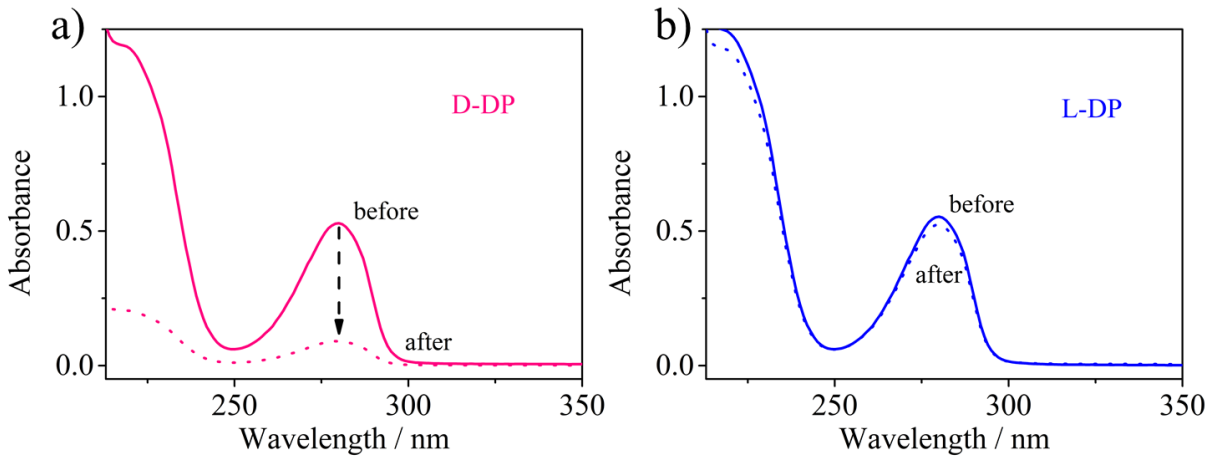

Figure S26. UV-vis spectra of (a) D-DP and (b) L-DP solutions before and after absorption employing DPFEG-GO membrane.

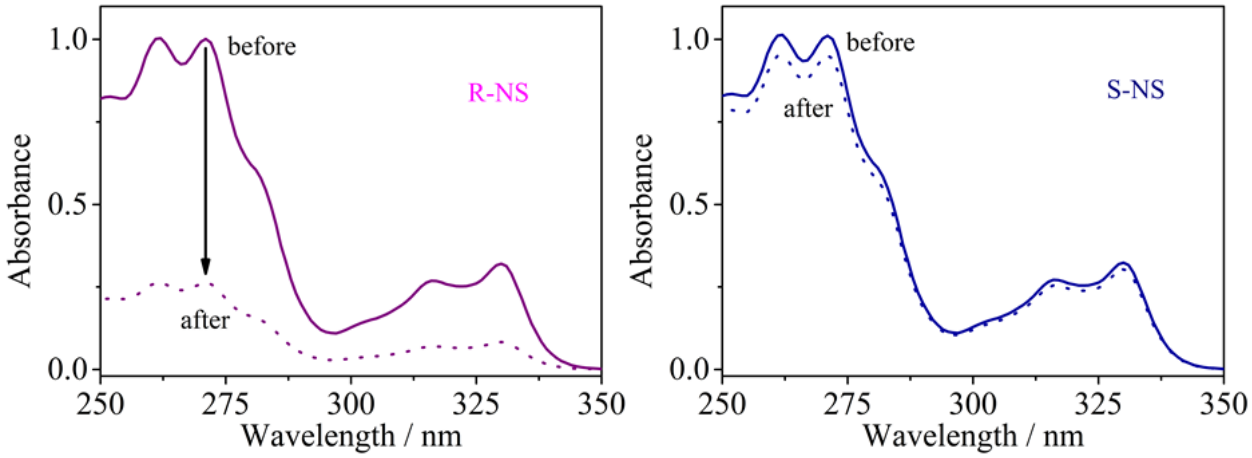

Figure S27. UV-vis spectra of (a) R-NS and (b) S-NS solutions before and after absorption employing DPFEG-GO membrane.

S18. Standard calibration curves of DP and NS

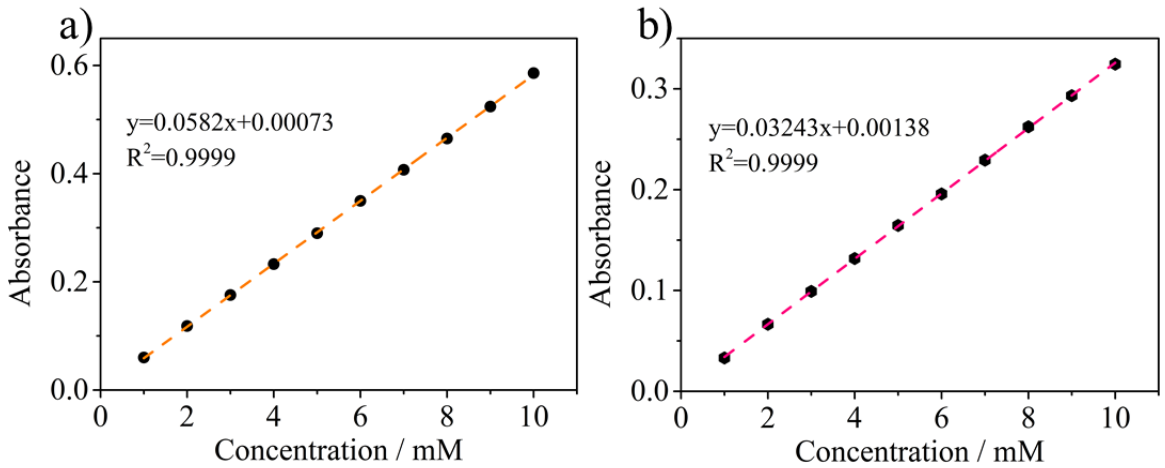

Figure S28. Linear relationship between the UV-vis response and concentration of DP (a) and NS (b).

S19. UPLC chromatograms of DP and NS

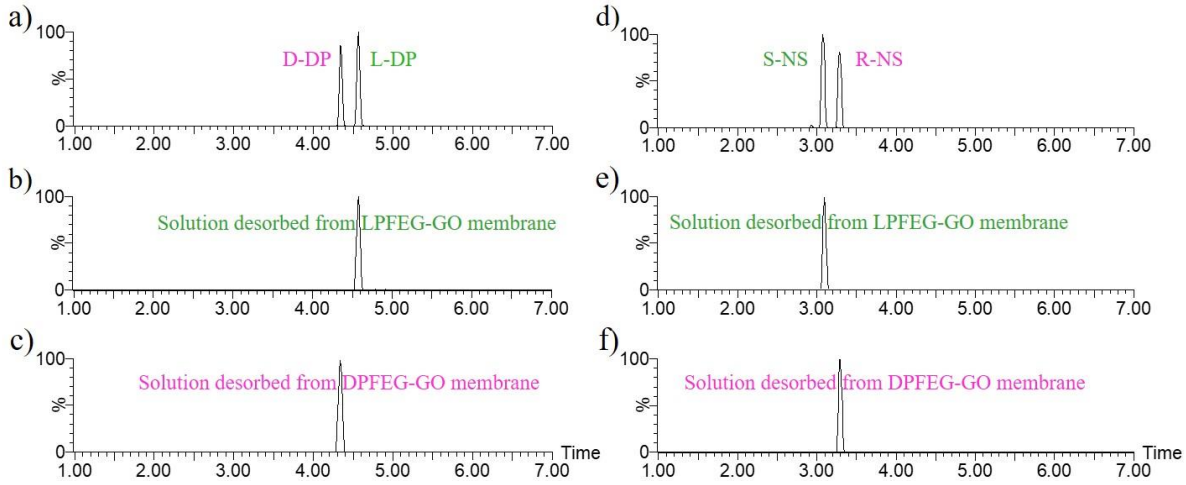

Figure S29. UPLC chromatograms of DP (a) and NS (d) racemates, and the corresponding solution desorbed from LPFEG-GO (b, e) and DPFEG-GO (c, f) membrane.

S20. The release of S-NS from LPFEG-GO membrane

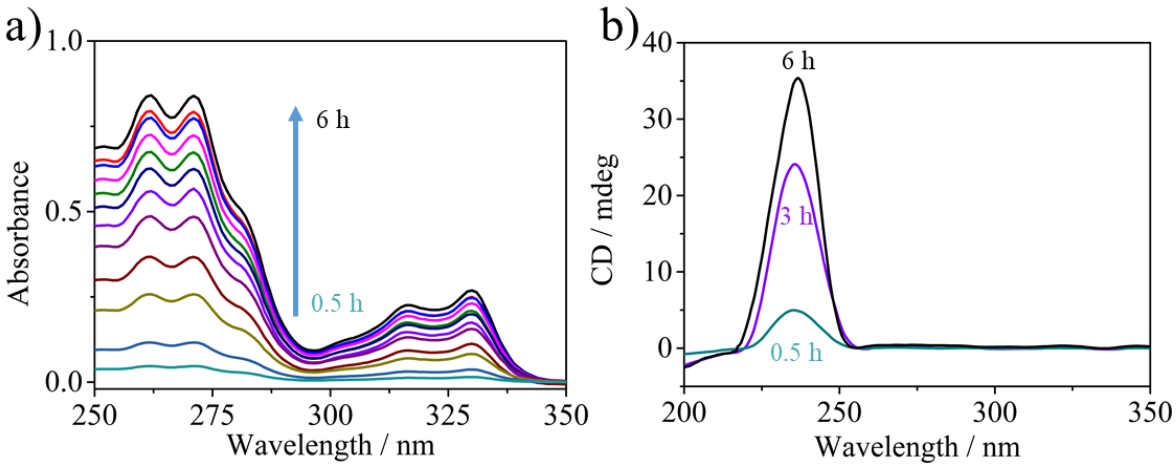

Figure S30. (a) UV-vis detection of released S-NS from LPFEG-GO membrane under different irradiation time. (b) The corresponding CD spectra of the release medium under UV light irradiation with time.

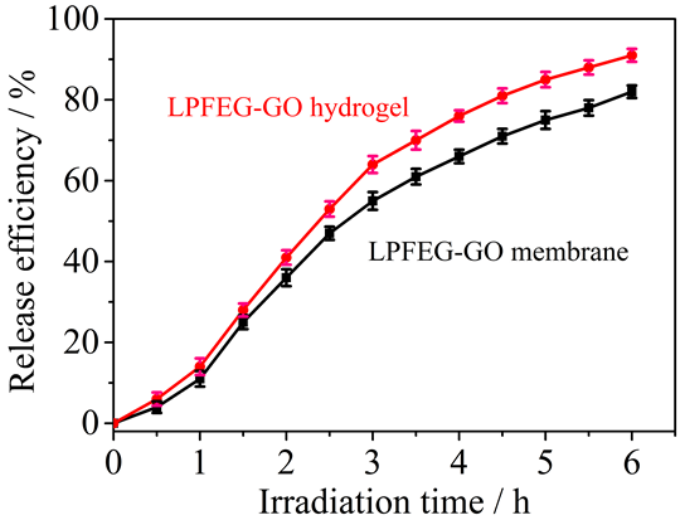

Figure S31. The amount of S-NS released from LPFEG-GO membrane (black line) and LPFEG-GO hydrogel (red line) at different time points.

S21. Photographs of LPFEG-GO hydrogel

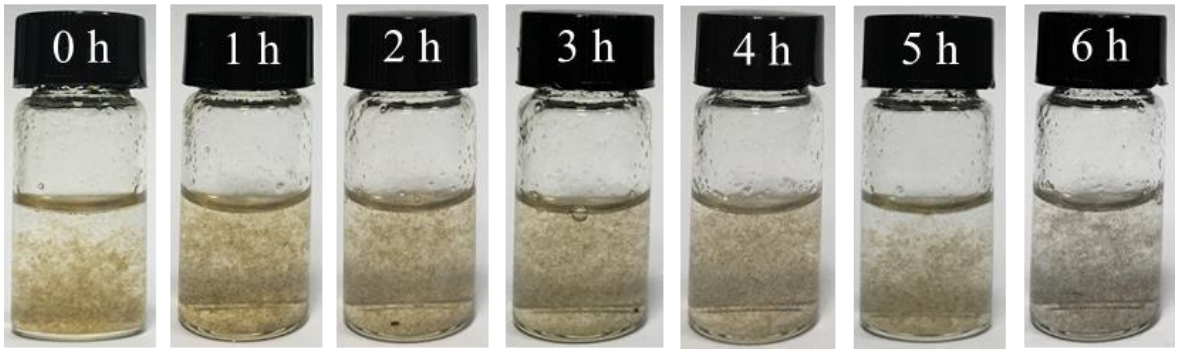

Figure S32. Time-dependent changes in LPFEG-GO hydrogel employing for drug-release process.

S22. Rheological properties

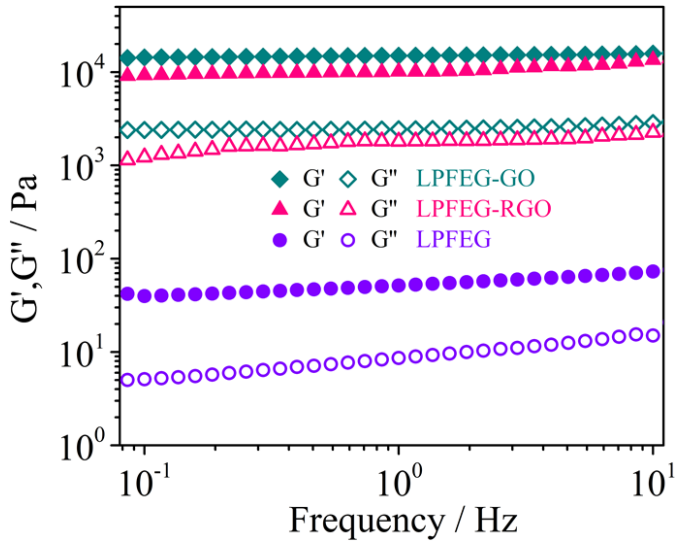

Figure S33. Rheological properties of the LPFEG, LPFEG-GO and LPFEG-RGO hydrogels.

S23. Chiroptical spectra of DP using L/DPFEG hydrogels for absorption

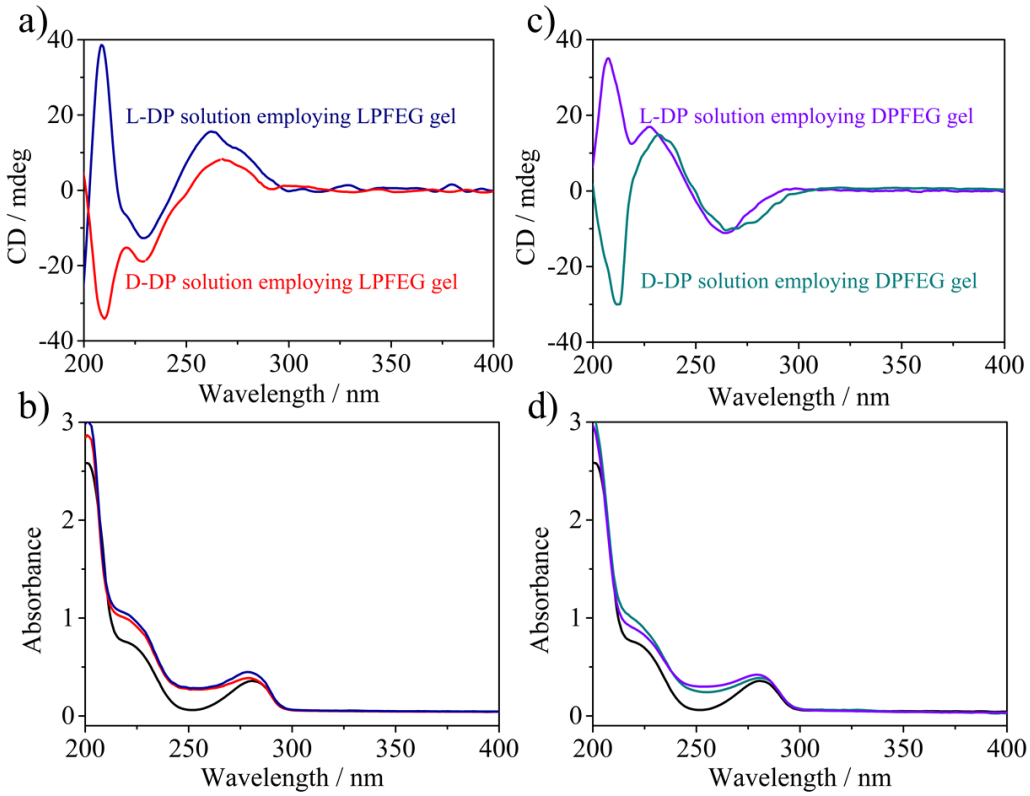

Figure S34. CD (a, c) and corresponding UV-vis spectra (b, d) of L-DP and D-DP systems after absorption employing LPFEG (a, b) and DPFEG hydrogels (c, d).

SUPPLEMENTARY METHODS

AFM and TEM image analysis. The surface morphologies and thickness of GO were characterized by AFM and TEM. The thickness of GO sheets were measured to be ~1.01 nm, indicating that they have a single-layer nanostructure. The GO sheets have comparable lateral dimensions in the range of several hundreds of nanometers to several micrometers according to their AFM and TEM images.

FTIR spectrum analysis. The FTIR spectrum of GO demonstrated the following characteristic functional groups of GO: C-O-C (~1052 cm^{-1}), C-O (1226 cm^{-1}), C-C (~1621 cm^{-1}) and C=O (1733 cm^{-1}) bonds.[1] The O-H stretching vibrations in the region of 3600-3300 cm^{-1} were attributed to the hydroxyl and carboxyl groups of GO and residual water between GO sheets.[2] These hydrophilic oxygen-containing functional groups provided GO sheets with a good dispersibility in water.

XRD spectrum analysis. A sharp and strong diffraction peak at $2\theta = 10.9°$ with d-spacing of 0.82 nm was observed in XRD spectrum, which is a characteristic peak supporting the existence of GO.[3] With the increase of irradiation time, the characteristic peak (10.9 °) gradually shifted towards a higher degree, suggesting that the oxygen-containing functional groups were partially reduced and the laminar channels became narrower. Moreover, the peak intensity decreased as a linear function of reduction time, which indicated that the RGO layer became disorder after the removal of functional groups.[4] After UV irradiation for 6 h, the interlayer space of the laminar channel decreased from 8.2 to 6.3 Å.

Raman spectrum analysis. The Raman spectrum of GO showed the presence of a G-band at ~1590 cm^{-1} and a D-band at ~1345 cm^{-1}. the intense D peak along with a large bandwidth indicated the significant structural disorder in GO.[5] The overtone 2D-band at around 2681 cm^{-1} was ascribed to the presence of two photons with opposite momentum which was contributed by double resonance transitions.[6]

XPS spectrum analysis. The synthesized sample was studied by X-ray photoelectron spectroscopy (XPS) to evaluate the chemical states of various elements and the presence of functional groups. The survey scan spectra of GO showed mainly the presence of carbon and oxygen with trace amount of sulfur (1.64 wt%), which was caused by process contamination. C1s spectra of GO were deconvoluted into five peaks that related to C-C (nonoxygen ring), C-O (hydroxyl and epoxy carbon), C=O (carbonyl), O-C=O, and π-π* satellite bonds at 284.7, 286.9, 288.2, 289.3, and 291.1 eV, respectively. These results demonstrated that the oxygen-containing groups are very rich for GO.[7] The content of oxygen atoms is as high as 32.4% and the content of carbon not bonded to oxygen is only 36.3%.

TGA analysis. The Thermogravimetric analysis analysis was conducted to test the thermal stability and the

overall oxidation of GO. The TGA spectrum of GO showed major weight losses between 150 and 300 ℃, which ascribed to the thermal decomposition of unstable oxygen functional groups such as hydroxyl, carbonyl and carboxylic acid to yield CO, CO_2, and H_2O.[8] Between 400 and 900 ℃, a slower mass loss was detected and could be attributed to the removal of more stable oxygen functionalities and the combustion of carbon skeleton.[1,9]

SUPPLEMENTARY REFERENCES

[1] Li, C.; Shi, G. Three-Dimensional Graphene Architectures. *Nanoscale* **2012**, *4*, 5549-5563.

[2] Zhu, Y.; Murali, S.; Cai, W.; Li, X.; Suk, J. W.; Potts, J. R.; Ruoff, R. S. Graphene and Graphene Oxide: Synthesis, Properties, and Applications. *Adv. Mater.* **2010**, *22*, 3906-3924.

[3] Dikin, D. A.; Stankovich, S.; Zimney, E. J.; Piner, R. D.; Dommett, G. H.; Evmenenko, G.; Nguyen, S. T.; Ruoff, R. S. Preparation and Characterization of Graphene Oxide Paper. *Nature* **2007**, *448*, 457-460.

[4] Gupta, B.; Kumar, N.; Panda, K.; Kanan, V.; Joshi, S.; Visoly-Fisher, I. Role of Oxygen Functional Groups in Reduced Graphene Oxide for Lubrication. *Sci. Rep.* **2017**, *7*, 1-14.

[5] Kudin, K. N.; Ozbas, B.; Schniepp, H. C.; Prud'Homme, R. K.; Aksay, I. A.; Car, R. Raman Spectra of Graphite Oxide and Functionalized Graphene Sheets. *Nano Lett.* **2008**, *8*, 36-41.

[6] Chen, J.; Yao, B.; Li, C.; Shi, G. An Improved Hummers Method for Eco-Friendly Synthesis of Graphene Oxide. *Carbon* **2013**, *64*, 225-229.

[7] Stathi, P.; Gournis, D.; Deligiannakis, Y.; Rudolf, P. Stabilization of Phenolic Radicals on Graphene Oxide: An XPS and EPR Study. *Langmuir* **2015**, *31*, 10508-10516.

[8] Shen, J.; Hu, Y.; Shi, M.; Lu, X.; Qin, C.; Li, C.; Ye, M. Fast and Facile Preparation of Graphene Oxide and Reduced Graphene Oxide Nanoplatelets. *Chem. Mater.* **2009**, *21*, 3514-3520.

[9] Abdelkader, A. M.; Valles, C.; Cooper, A. J.; Kinloch, I. A.; Dryfe, R. A. Alkali Reduction of Graphene Oxide in Molten Halide Salts: Production of Corrugated Graphene Derivatives for High-Performance Supercapacitors. *ACS Nano* **2014**, *8*, 11225-11233.